Forces and Currents in Carbon Nanostructures: Are we imaging atoms? Supplementary Information

Martin Ondráček,[1] Pablo Pou,[2] Vít Rozsíval,[1] César González,[3] Pavel Jelínek,[1] and Rubén Pérez[2]

[1]*Institute of Physics, Academy of Sciences, Cukrovarnická 10, 162 00, Prague, Czech Republic*
[2]*Departamento de Física Teórica de la Materia Condensada, Universidad Autónoma de Madrid, E-28049 Madrid, Spain*
[3]*Instituto de Ciencia de Materiales de Madrid (ICMM-CSIC), E-28049 Madrid, Spain*

(Dated: March 9, 2011)

I. IMAGE PATTERNS FOUND IN SCANNING PROBE MICROSCOPE (SPM) EXPERIMENTS.

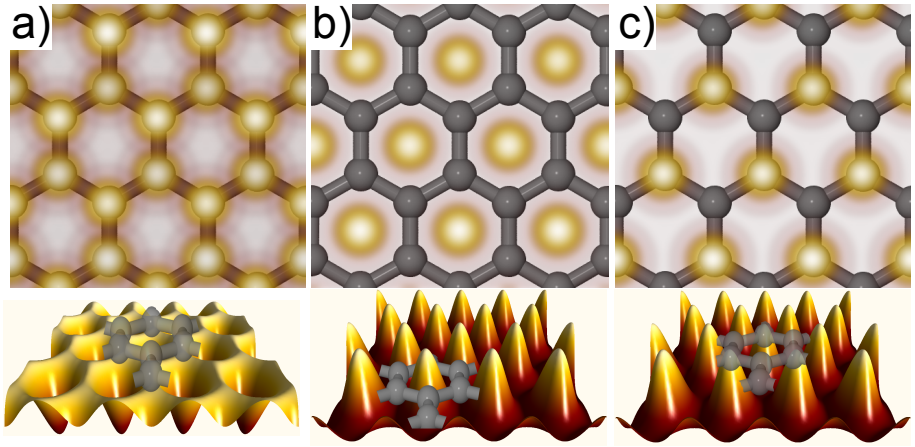

FIG. 1: **Image patterns found in SPM experiments.** Topographic STM (AFM) images reflect the displacement of the tip to keep the current (force) constant while scanning over the surface. Bright spots correspond to positions with the largest currents (forces) and, thus, to the highest retraction (largest tip-sample distance). **(a)** Maximal currents (forces) on the carbon atoms produce a honeycomb pattern of bright spots matching the underlying atomic structure. A hexagonal pattern is consistent with current (force) maxima either on three (the C_β) of the six atoms in the ring **(c)** or on the hollow sites **(b)**.

II. FIRST-PRINCIPLES CALCULATIONS FOR FORCES AND CURRENTS: METHODOLOGICAL DETAILS

We have calculated force vs distance curves for different tip apex models over a carbon nanotube (NT) and a graphite(0001) surface. The (17,0) Single Wall Carbon Nanotube (SWCNT) mimics well the properties of the nanotubes used in the experiments[1]: it is semiconducting and has a diameter of 13.34 Å (experimental estimate: 13.38 Å), but requires a significant smaller unit cell for the simulations. We have used a cubic supercell that includes three primitive cells of the (17,0) SWCNT unit cell (204 atoms), and a vacuum of, at least, ∼7 Å in the directions perpendicular to the SWCNT axis, with a final size of 22 Å × 12.78 Å × 33 Å (y corresponds to the SWCNT axis and z to the tip approaching direction). We have fixed the 12 atoms at the bottom of the NT and the top layer of the apex model. The graphite surface has been simulated using a 6×6 unit cell (containing 72 atoms), fixing the position of the second C-layer and the four carbon atoms on the surface which are – within the supercell – the most distant ones from the tip.

Our Density Functional Theory (DFT) calculations use a standard implementation with a plane wave basis set (VASP[2]). We use the projector-augmented plane wave method (PAW)[3] for the SWCNT calculation and Vanderbilt ultra-soft pseudopotential (US-PP) method for the calculations with graphite (graphene). We set the plane wave cutoff to 500 eV for PAW and to 287 eV for US-PP. We have checked for one particular case, namely for a graphene bilayer with the Si-dimer tip positioned over the C_α atom, that the forces calculated with the US-PP do not substantially differ from those obtained with the PAW method (the difference is typically between 0.01 and 0.02 nN). The $\vec{k}$-sampling is done with a Monkhorst-Pack (MP) mesh of $1 \times 4 \times 1$ for the SWCNT and $2 \times 2 \times 1$ for the graphite. The tip-sample interaction is calculated with a quasistatic approach: for a given tip-surface distance, all the free atoms in the supercell are relaxed to the ground state, and DFT and vdW energies are determined. Then, we further approach the tip to the sample by 0.25 Å and repeat the procedure. Forces are extracted from a numerical derivative of the energy vs distance curves. The convergence criteria for the atomic relaxations are 10^{-6} eV for the total energy and 0.01 eV/Å (SWCNT) or 0.001 eV/Å (graphene) for the maximum value of the forces on the free atoms.

We have used the semi-empirical approach by Grimme[4] for the van der Waals (vdW) calculations. In this method, vdW interactions are described by London dispersion forces with parameters fitted to reproduce high-level quantum chemistry calculations for molecules containing elements up to Z=54 (Xe). For W (Z=74), we have used the method proposed by Eltsner et al.[5] that is based on the use of atomic or bulk polarizabilities. In both theories the vdW

energy is calculated as a sum of pairwise potentials, $E_{vdW} = \sum_{i,j} f(R_{i,j}) C^{(6)}_{i,j} / R^6_{i,j}$, where $f(R_{i,j})$ is a dumping function that suppresses the vdW interaction at interatomic separations around the bonding distance. Notice that for these calculations we do not use a supercell approach: we calculate explicitly the interaction of a single tip with an infinite nanotube or graphene plane. Both vdW semiempirical approaches yield the same qualitative results.

The calculation of STM currents is based on nonequilibrium Keldysh-Green function techniques and the details of the implementation are presented in Ref. 6. The tip is described by a 5-atom tungsten pyramid attached to a (100)-oriented 4-layer W slab. The sample is a graphene bilayer with a 3×3 surface periodicity. In order to get an accurate description of the graphite electronic properties, a MP mesh with 1024 points is used to sample the 2D Brillouin zone.

III. SHORT-RANGE CHEMICAL FORCES AND VDW CONTRIBUTIONS FOR ALL THE TIPS CONSIDERED IN OUR STUDY.

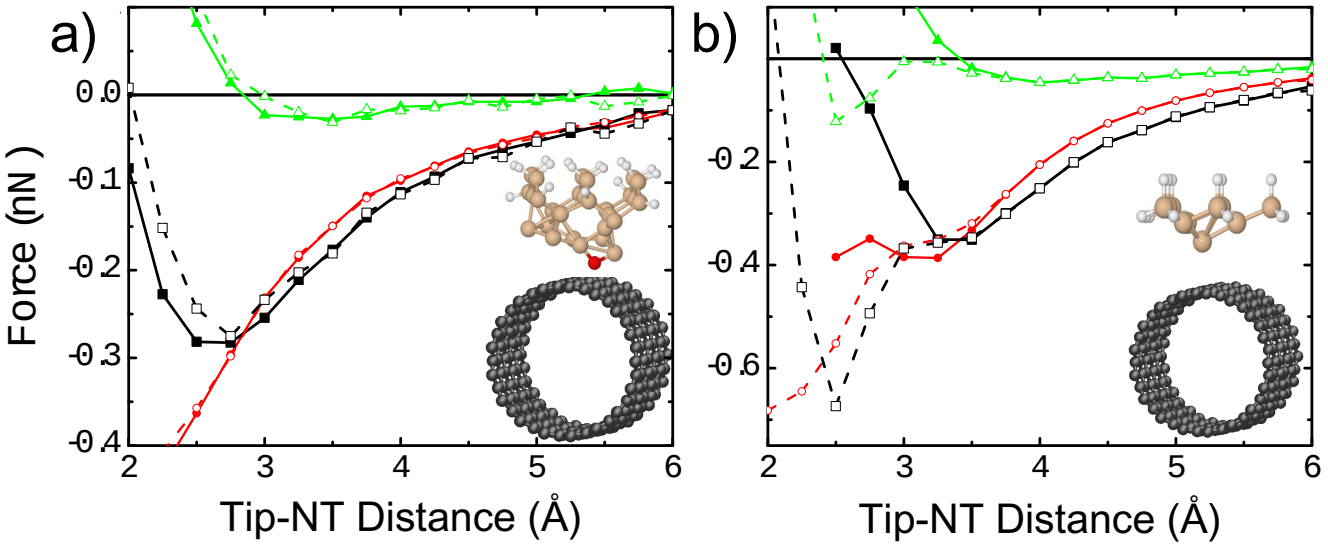

FIG. 2: **Short-range chemical force versus van der Waals interaction on the CNT with tips of different chemical reactivity.** Forces as a function of the tip-nanotube distance for a (17,0) single wall carbon nanotube interacting with **(a)** the oxygen-terminated Si tip and **(b)** the more reactive H3 Si tip. The tip apex is located over the hollow site (solid symbols) and over a carbon atom (open symbols). The total force (GGA+vdW, black squares) is a combination of the microscopic vdW interaction calculated with a semi-empirical approach (vdW, red circles) and the short-range chemical interaction described by density functional theory with a gradient-corrected exchange-correlation functional (PBE GGA, green triangles).

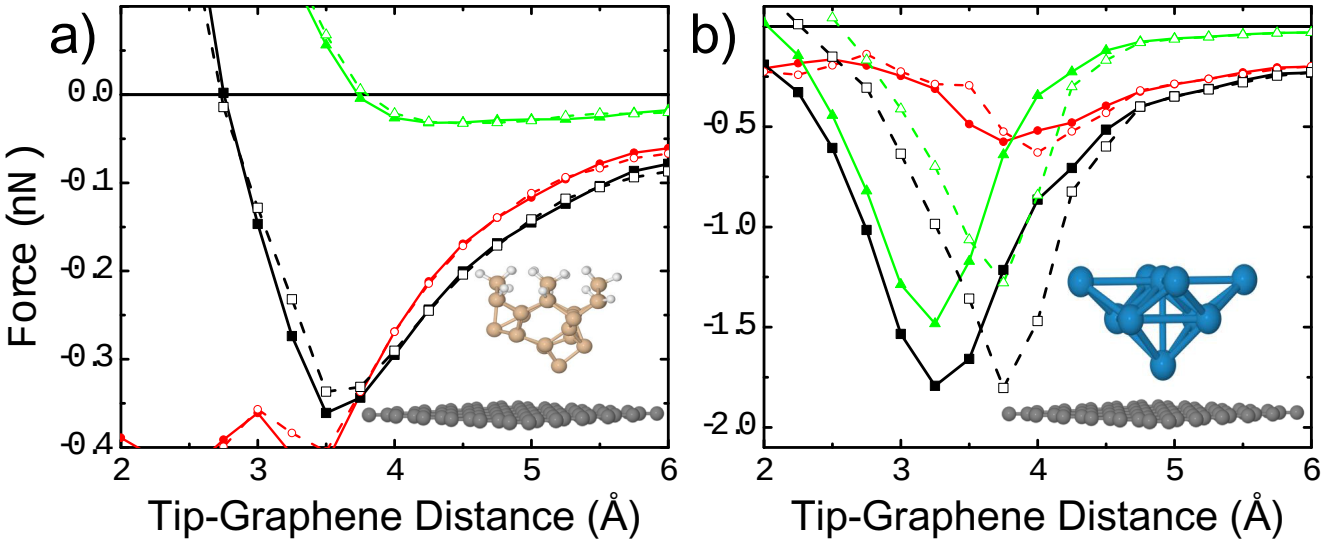

FIG. 3: **Short-range chemical force versus van der Waals interaction on the (0001) graphite surface with tips of different chemical reactivity.** The graphite surface is modeled by a simple graphene layer. The forces as a function of the tip-sample distance are calculated over the hollow position (solid symbols) and the carbon atom (open symbols) for a dimer terminated Si tip **(a)** and a metallic W tip **(b)**. Forces calculated with GGA (green triangles), van der Waals (red circles) and also the total force, GGA+vdW (black squares) are shown.

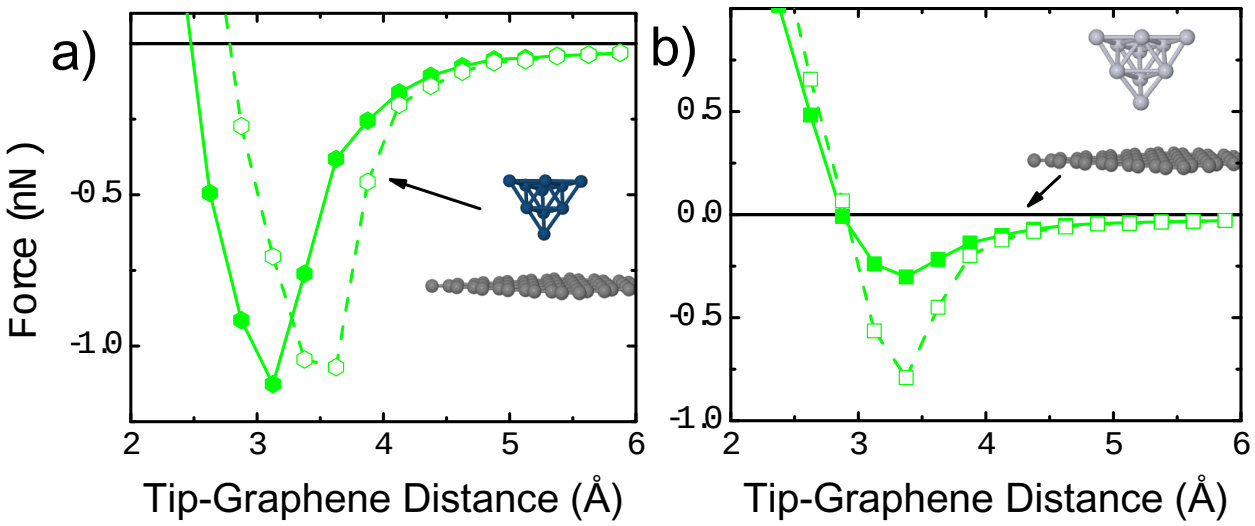

FIG. 4: **Short-range chemical force on the (0001) graphite surface with tips of different chemical composition.** The graphite surface is modeled by a simple graphene layer. The forces as a function of the tip-sample distance are calculated over the hollow position (solid symbols) and the carbon atom (open symbols) for an Ir tip **(a)** and a Pt tip **(b)**. Only forces calculated with GGA (green triangles) are shown.

IV. LOCAL DENSITY APPROACH (LDA) VERSUS GENERALIZED GRADIENT APPROACH PLUS VAN DER WAALS (GGA+VDW) CALCULATIONS.

It is well known that the LDA approximation[7] to the exchange-correlation functional overestimates the chemical interaction. This error seems to be more important in weakly interacting systems. GGA functionals (and, in particular, PBE[8]) provide a better description but they lack a proper treatment of the vdW interaction. Previous calculations have shown that the LDA overbinding can reproduce quite nicely the result of more sophisticated GGA+vdW (PBE+vdW) calculations. This is, for example, the case of the interplane spacing in graphite, where LDA provides a very good estimate. Figures 5 and 6 compare the LDA and GGA+vdW forces for the SWCNT and graphite. For weakly reactive tips, while GGA calculations do not provide any significant attraction, LDA forces are similar to the GGA+vdW ones, yielding maximum attractive forces of the order of the experimental ones. Although the exponential decay for large distances is different from the $1/R^{\alpha}$ dependence shown by the total van der Waals interaction between the apex model and the whole sample, the equilibrium distances and maximum attractive forces obtained with LDA better reproduce the experimental evidence than GGA results alone. Force differences between different sites are reasonably well reproduced. In the case of metallic tips, where the vdW contribution is not so relevant, LDA overestimates the interaction and favours particularly the positions on top of the atoms.

V. MULTIPLE SCATTERING EFFECTS IN THE STM CURRENTS AND CONTRAST INVERSION IN THE NEAR-CONTACT REGIME.

Tunneling currents are essentially controlled by the density of states of the tip and sample and by the the hopping matrix elements that couple them. Under normal operation conditions, the tip-sample distance lies in the 5-10 Å range. At these distances, the hopping matrix elements are still small (they have an exponential distance decay) and theoretical studies can be carried out with perturbative approaches like the Bardeen Tunneling theory[9], that essentially applies the Fermi Golden rule (first order time-dependent perturbation theory) to this problem. According to this approach, the tunneling current is proportional to the square of the hoppings. The popular Tersoff-Hamman theory is a further simplification of the Bardeen theory where drastic approximations are made on number and shape of tip wavefunctions available for tunneling[10,11]. Apart from the direct tunneling event described by Bardeen theory, there are other processes that contribute to the tunneling current when multiple scattering suffered by the electrons flowing between the tip and the sample starts playing a role[6]. In these higher-order processes, the electron, instead of tunneling directly, moves back and forth between the tip and the sample several times. The contribution of the higher-order processes is proportional to increasingly larger powers of the hopping elements and they thus can be neglected for large tip-sample distances. However, upon approaching the tip to the sample, they become relevant and first order approaches are not valid anymore: the contributions to the transmission matrix have to be calculated at all orders[6]. Our non-equilibrium Green's function formulation incorporates naturally these effects through a resummation of all the processes, which results in an effective hopping matrix.

These multiple scattering effects lead to the saturation of the current at small tip-sample distances and to conductance quantization upon reaching the contact[12]. We have already used this approach, together with the atomic

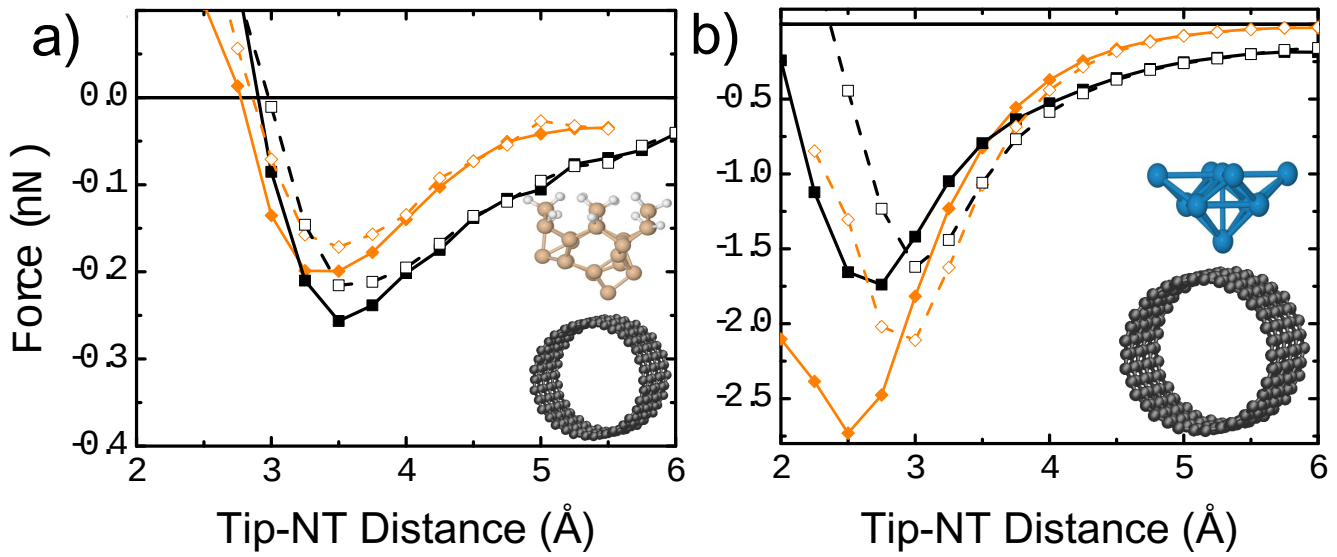

FIG. 5: **LDA vs GGA+vdW force curves for a (17,0) SWCNT.** LDA (orange diamonds) and GGA+vdW (black squares) forces as a function of the tip-sample distance are calculated over the hollow position (solid symbols) and the carbon atom (open symbols) with a Si dimer tip (a) and a W tip (b).

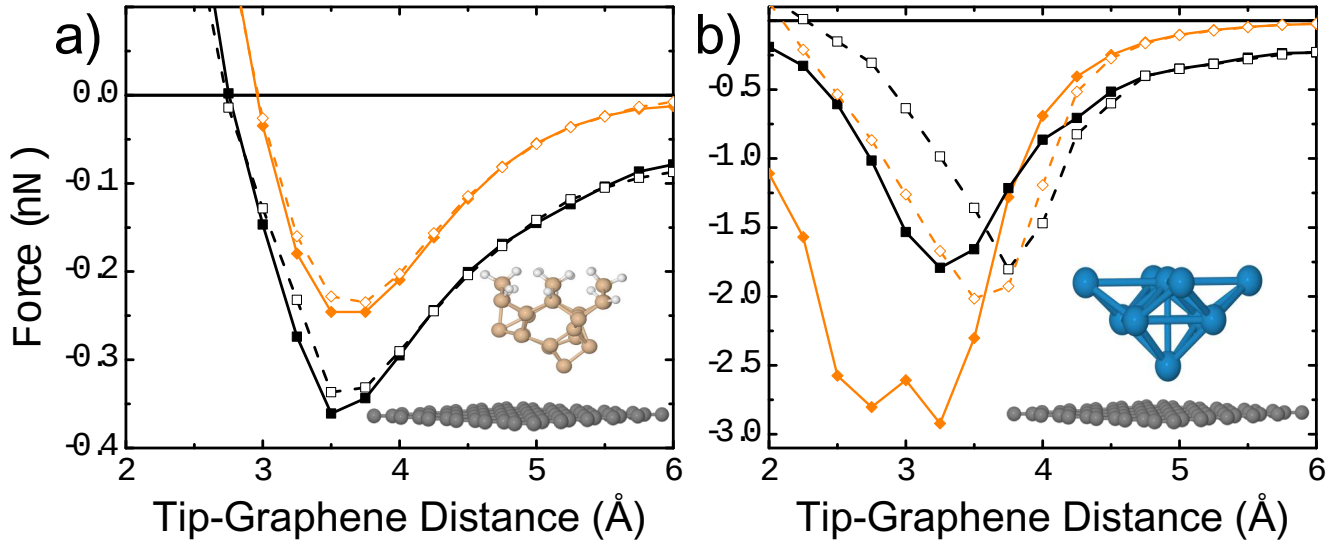

FIG. 6: **LDA vs GGA+vdW force curves for a (0001) graphite surface modeled with one graphene layer.** LDA (orange diamonds) and GGA+vdW (black squares) forces as a function of the tip-sample distance are calculated over the hollow position (solid symbols) and the carbon atom (open symbols) with a Si dimer tip (a) and a W tip (b).

relaxations induced by the tip-sample interaction, to explore the final stages of the breaking of metallic nanocontacts, the origin of the atomic resolution in closed-packed metal surfaces (where the interplay between atomic relaxations and current saturation plays a crucial role in determining the observed corrugation)[12] and the surprising drop in the current on semiconductor surfaces when approaching the contact[13].

The multiple scattering effects are responsible for inversion of the contrast in graphite for distances below ~ 4 Å. Figure 7 shows the evolution of the current with the distance over an atom and the hollow site including or not the multiple scattering effects. No atomic relaxation induced by the tip-sample interaction has been included in these calculations. As shown in Figure 7, the current starts to saturate on top of the carbon atoms while it is still growing on the hollow site, leading to a crossing that explains the contrast inversion. Images taken in the close- and far-distance regimes would show hexagonally arranged maxima, but the maxima would correspond to hollow or atomic sites respectively. First-order perturbative approaches, like the ones used so far for the study of graphite[14–17] fail to capture this behaviour. In contrast to other surfaces, graphite is very compliant in the normal direction due to the weak coupling between graphene planes. Even the vdW tip-sample interaction, that is quite large for the blunt metal tips used in STM experiments, is enough to deform the upper surface layers and lead to real tip-surface distances in the range where multiple scattering effects are relevant, even when experiments are performed at nominally large separations. This would explain the most common hexagonal pattern found in the experiments, even when performed

at bias voltages where, in the tunneling regime, both atoms in the unit cell should be imaged and the honeycomb structure revealed.

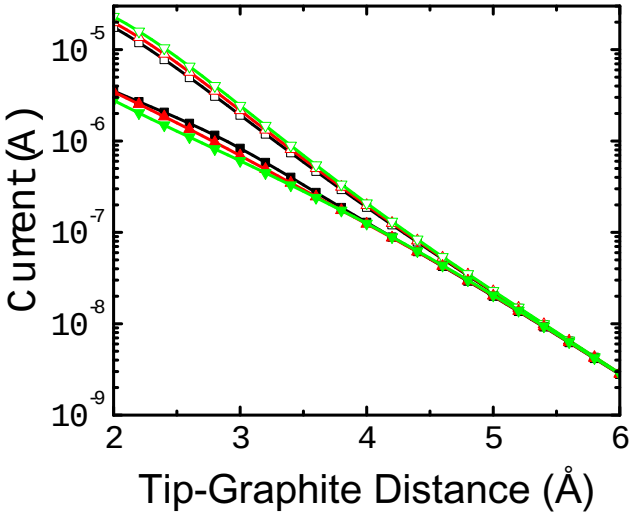

FIG. 7: **STM currents versus distance for the graphite(0001) surface with and without multiple scattering.** Currents at a bias voltage of -300 mV on top of the alpha and beta atoms (red and green triangles) and over the hollow site (black squares) including multiple scattering effects (solid symbols) and using only a first-order perturbative approach (open symbols).

VI. ATOMIC RELAXATION EFFECTS IN THE STM IMAGES.

Honeycomb-like STM images on HOPG have been reported by several groups[15,18–22]. In particular, Cisternas et al.[15] showed that STM hexagonal-like images evolve to honeycomb-like structures reducing the tip-sample distances even at low bias. A key feature to explain in detail these measurements could be the atomic relaxations induced by the tip-sample interaction[23]. The STM simulations presented in the letter do not involve the effect of these relaxations that are also required to perform a direct comparison between the force and the electronic current.

In order to illustrate qualitatively the influence of the atomic relaxations in the STM corrugation, we have performed calculations on graphite where we have modified the height of one of the carbon atoms in a range of 1-10 pm and computed the corresponding constant height STM profiles (see Fig. 8). These displacements mimic the atomic relaxations induced by the tip-sample interaction when the tip is on top of that atom in the attractive regime. In order to isolate the effect of the atomic relaxations, we use in these calculations a model tip including only a dz^2 orbital and consider a tip-surface distance of 5Å where multiple-scattering effects are not relevant.

Due to the high surface atomic density, the STM current at any tip position is not dominated by a single surface atom but it is shared by several neighboring atoms (1+3 1st neighbors at top positions, 6 at the hollow site). This effect produces the low corrugation showed in our calculations (see Fig. 3 in the letter). The new results (see Fig. 8) show that the atomic relaxations, even for small displacements, clearly enhance the atom-hollow corrugation favoring STM honeycomb patterns in the attractive regime as the tip-surface interaction produces a larger reduction of the tip-surface distance when the tip is placed over the atoms. However, as we reported in our letter, at the near-contact regime, the attraction is larger over the hollow positions (see Fig. 2 in the letter) and, for the W tip, the multiple scattering has already induced the contrast inversion at these tip-surface distances. Therefore, in the near-contact regime, multiple-scattering effects and tip-induced atomic relaxations work together: atomic relaxations would enhance the contrast but producing, at this regime, more corrugated "hexagonal"-like images. Under normal STM operation conditions, considering the low normal stiffness of graphite and the typical tip radius for metal tips of 20-50 nm (that results in a large vdW interaction), it is difficult to reach the pure attractive regime. However, it can be probably accessed in experiments where intentionally different tip-surface distance ranges are carefully explored (like those in ref. 15), giving rise to the observation of honeycomb motifs reported in the literature.

We notice that, in the transition between these two regimes, there is an intermediate distance range where both effects, multiple scattering and atomic relaxations, are, in principle, relevant but tend to produce opposite effects. The exact STM pattern can be very complex and would depend on the interplay of the particular tip structure and electronic properties as they control both (i) the tip-sample interactions, and (ii) the tip density of states and hopping matrix elements that influence the tunneling currents. In combined AFM/STM experiments probing this intermediate regime, we cannot discard the appearance of patterns where AFM and STM images may be shifted as reported in ref. 24.

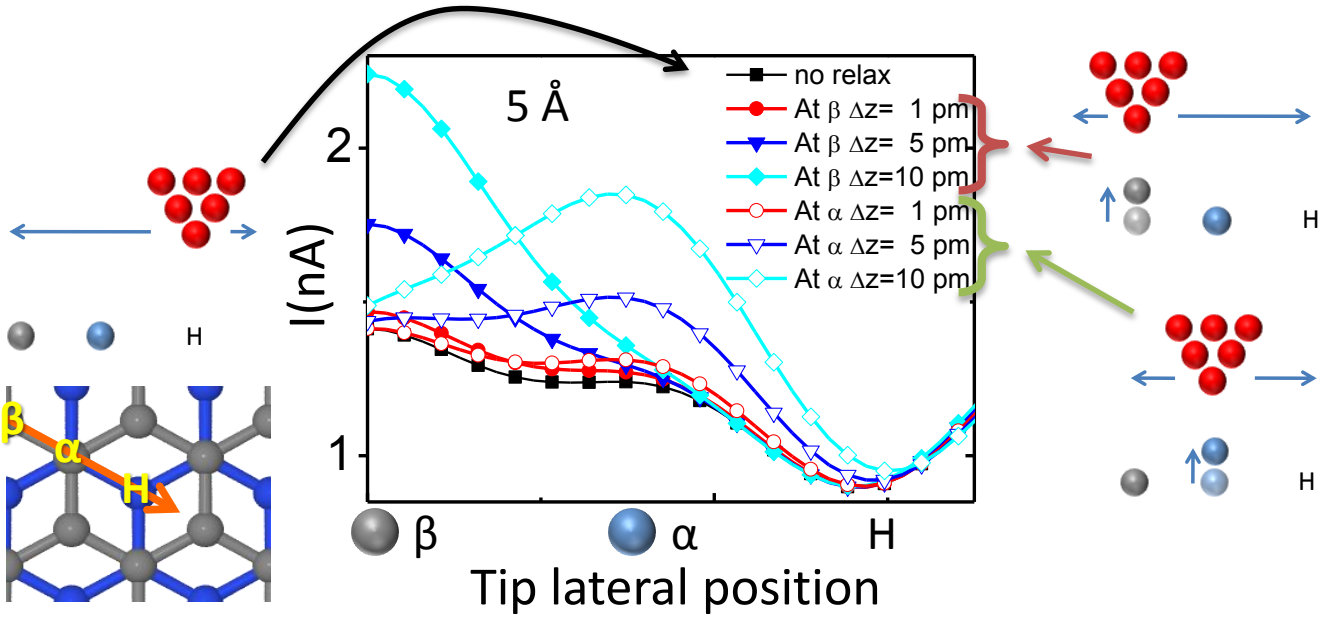

FIG. 8: **STM currents profiles for the graphite(0001) surface with and without atom displacements.** STM constant height (5 Å) current profiles, along the beta-alpha-hollow line, calculated with fixed atom positions apart from a normal displacement (from 1 pm to 10 pm) of the alpha or beta carbon atom towards the tip. These displacements mimic the atomic relaxations induced by the tip-sample interaction when the tip is on top of that atom in the attractive regime. In order to isolate the effect of the atomic relaxations, we use in these calculations a model tip including only a dz^2 orbital and consider a tip-surface distance of 5 Å where multiple-scattering effects are not relevant. Bias voltage is set at -0.3 eV. The rest of the computational parameters are the same as in the previous STM calculations. Notice that small displacements significantly increase the current over the position of the atoms. These results show that the atomic relaxations, even for small displacements, clearly enhance the atom-hollow corrugation favoring STM honeycomb-like patterns in the attractive regime as the tip-surface interaction produces a larger reduction of the tip-surface distance when the tip is placed over the atoms.

[1] M. Ashino, A. Schwarz, T. Behnke, and R. Wiesendanger, Phys. Rev. Lett. **93**, 136101 (2004).
[2] G. Kresse and J. Furthmller, Phys. Rev. B **54**, 11169 (1996).
[3] G. Kresse and D. Joubert, Phys. Rev. B **59**, 1758 (1999).
[4] S. Grimme, Journal of Computational Chemistry **25**, 1463 (2004).
[5] M. Elstner, P. Hobza, T. Frauenheim, S. Suhai, and E. Kaxiras, Journal of Chemical Physics **114**, 5149 (2001).
[6] J. M. Blanco, F. Flores, and R. Pérez, Progress in Surface Science **81**, 403 (2006).
[7] J. P. Perdew and A. Zunger, Phys. Rev. B **23**, 5048 (1981).
[8] J. P. Perdew, K. Burke, and M. Ernzerhof, Phys. Rev. Lett. **77**, 3865 (1996).
[9] J. Bardeen, Phys. Rev. Lett. **6**, 57 (1961).
[10] J. Tersoff and D. R. Hamann, Phys. Rev. Lett. **50**, 1998 (1983).
[11] J. Tersoff and D. R. Hamann, Phys. Rev. B **31**, 805 (1985).
[12] J. M. Blanco, C. González, P. Jelínek, J. Ortega, F. Flores, and R. Pérez, Physical Review B **70**, 085405 (2004).
[13] P. Jelínek, M. Švec, P. Pou, R. Pérez, and V. Cháb, Physical Review Letters **101**, 176101 (pages 4) (2008).
[14] S. Hembacher, F. J. Giessibl, J. Mannhart, and C. F. Quate, Proceedings of the National Academy of Sciences of the United States of America **100**, 12539 (2003).
[15] E. Cisternas, F. Stavale, M. Flores, C. A. Achete, and P. Vargas, Physical Review B **79**, 205431 (2009).
[16] D. Tománek and S. G. Louie, Phys. Rev. B **37**, 8327 (1988).
[17] D. Tománek, S. G. Louie, H. J. Mamin, D. W. Abraham, R. E. Thomson, E. Ganz, and J. Clarke, Physical Review B **35**, 7790 (1987).
[18] H. A. Mizes, S.-i. Park, and W. A. Harrison, Phys. Rev. B **36**, 4491 (1987).
[19] P. J. Ouseph, T. Poothackanal, and G. Mathew, Physics Letters A **205**, 65 (1995).
[20] J. I. Paredes, A. Martinez-Alonso, and J. M. D. Tascon, Carbon **39**, 476 (2001).
[21] Y. Wang, Y. Ye, and K. Wu, Surface Science **600**, 729 (2006).
[22] G. S. Khara and J. Choi, Journal of Physics: Condensed Matter **21**, 195402 (2009).
[23] J. M. Soler, A. M. Baro, N. García, and H. Rohrer, Phys. Rev. Lett. **57**, 444 (1986).
[24] S. Hembacher, F. J. Giessibl, J. Mannhart, and C. F. Quate, Phys. Rev. Lett. **94**, 056101 (2005).